



1 Taklimakan Desert Nocturnal Low Level Jet: Climatology and Dust Emission

2 Ge J.M.¹, H.Y. Liu^{1,3}, J.P. Huang^{1,*}, and Q. Fu^{1,2}

3 ¹Key Laboratory for Semi-Arid Climate Change of the Ministry of Education and

4 College of Atmospheric Sciences, Lanzhou University, Lanzhou, 730000, PRC

5 ²Department of Atmospheric Sciences, University of Washington, Seattle, WA, 98105,

6 USA

7 ³Hebei Province Meteorological Service Center, Shijiazhuang, 005021, PRC

8

9

10

11

12

13

14

15

16

17

18 Submitted to *Atmos. Chem. and Phys.*

19 hjp@lzu.edu.cn

20 March 2016



21

Abstract

22 While nocturnal Low-Level Jets (NLLJs) occur frequently in many parts of the
23 world, the occurrence and other detailed characteristics of NLLJs over the Taklimakan
24 Desert (TD) are not well known. This paper presents a climatology of NLLJs and
25 coincident dust over the TD by analyzing multi-year ERA-Interim reanalysis and
26 satellite observations. It is found that the ERA-Interim dataset can capture the NLLJs
27 feature well by comparing with radiosonde data from two surface sites. The NLLJs
28 occur in more than 60% of nights, which are primarily easterly to east-northeasterly.
29 They typically appear at 100 to 400 m above the surface with a speed of 4 to 10 ms⁻¹.
30 Most NLLJs are located above the nocturnal inversion during warm season while they
31 are embedded in the inversion layer during cold season. NLLJs above the inversion
32 have a strong annual cycle with a maximum frequency in August. We also quantify
33 the convective boundary layer (CBL) height and construct an index to measure the
34 magnitude of the momentum in the CBL. We find that the NLLJ contains more
35 momentum than without NLLJ, and in warm season the downward momentum
36 transfer process is more intense and rapid. The winds below the NLLJ core to the
37 desert surface gain strength in summer and autumn, which are coincident with an
38 enhancement of aerosol optical depth. It indicates that the NLLJ is an important
39 mechanism for dust emission and transport during the warm season over the
40 Taklimakan.

41 Key words: Taklimakan Desert, Low-level Jet, Boundary, Dust Aerosol

42



43 1. Introduction

44 The Taklimakan Desert (TD) is one of the largest deserts and located farther
45 from an ocean than any other desert in the world. It occupies the central part of the
46 Tarim Basin in northwestern China, extending about 1000 km from east to west and
47 400 km from north to south (Figure 1) with an extremely dry continental climate
48 [Huang *et al.*, 2015]. Most of the TD area is composed of shifting sand dunes and it is
49 the most intense dust aerosol source in Asia. The TD is of particular interest not only
50 because of its large contribution to the global dust emission, but also because of its
51 very unique orography and prevailing winds. The prevailing wind direction in the low
52 level atmosphere of the TD is easterly and northeasterly (Figure 1), which is
53 consistent with the dominant direction of motion of the sand dunes. The elevation of
54 the TD is about 0.8 km above sea level (ASL) at the northeast side of the Tarim basin,
55 increasing gradually to 1.5 km ASL at the southwest area. The basin is open on its
56 eastern side while the other three sides are surrounded by the high relief of mountains
57 and plateaus with an average elevation over 4.5 km. The prevailing northeasterly,
58 low-altitude winds limit the flow of low-level dust out of this region much of the time.
59 However, former studies have indicated that dust from the TD can be lofted above 5
60 km into the upper troposphere [Huang *et al.*, 2007, Ge *et al.*, 2014], and subsequently
61 transported over long distances and around the globe by the westerlies [Uno *et al.*,
62 2009]. This long-lasting dust aerosol can perturb the energy balance of the
63 earth-atmosphere system through its direct radiative effects on solar and terrestrial
64 radiation [Huang *et al.*, 2014; Fu *et al.*, 2009; Ge *et al.*, 2010; 2011], indirect



65 radiative effects via its influence on physical properties of clouds [Lohmann &
66 Feichter, 2005; Su *et al.*, 2008; Huang *et al.*, 2014], and semi-direct effects by
67 heating the dust layer [Huang *et al.*, 2009; 2014]. Thus, high concentrations of
68 elevated dust and its long range transport from the Taklimakan may play an important
69 role in climate and climate change [Huang *et al.*, 2008; Ling *et al.*, 2014]. To better
70 understand dust emission, transport and the influence on climate will require more
71 exploration of the local and meso-scale meteorological processes over this dust source
72 region.

73 Dust emission processes are controlled by meteorology and surface properties,
74 such as surface wind, soil texture, moisture content, surface roughness and vegetation.
75 A surface wind that exceeds a particle-size-dependent speed threshold is a condition
76 for dust resuspension [Shao *et al.*, 2011]. Above the threshold the dust emission flux
77 is highly sensitive to wind speed [Chen *et al.*, 2013]. Synoptic scale frontal incursions
78 and cold air outbreaks are known to lead to strong surface winds, resulting in dust
79 storms over the Taklimakan and Gobi deserts [Sun *et al.*, 2001]. Another mechanism
80 that can lead to strong surface winds in semi-arid and desert regions is through the
81 formation of a Nocturnal Low-Level Jet (NLLJ) [Fiedler *et al.*, 2013; Rife *et al.*,
82 2010].

83 NLLJ are generally characterized as a relatively thin layer with highest wind
84 speeds in a core between 300 and 600 meters above ground level (AGL) while there
85 are usually minima in wind speed 1.0 to 2.0 km above the core [Rife *et al.*, 2010]. A
86 diurnal cycle is a common and well documented feature of NLLJ with onset and



87 cessation times generally in the early evening and mid-morning, respectively.
88 Maximum speeds occur around 0000 to 0300 local time. Nocturnal low-level jets with
89 diurnal variability form primarily by two mechanisms. One mechanism is the forcing
90 by changes in baroclinicity associated with orographic channeling, temperature
91 gradients and frontal dynamics [*Baas et al.*, 2009; *Stensrud*, 1996; *Washington and*
92 *Todd*, 2005]. The other is related to the decoupling of jet winds from the surface, and
93 subsequent recoupling due to diurnally varying eddy viscosity and friction layer depth
94 that accompanies changes in inversion layer depth driven by surface thermal radiation
95 emission and solar heating. This is the initial oscillation mechanism (IO) as advanced
96 by Blackadar [1957] [*Van de Wiel et al.*, 2010]. The formation of NLLJs is favored
97 over relatively flat terrain in arid and semi-arid regions. When these essentially local
98 forcing mechanisms exist on a large scale over relatively uniform, level terrain such
99 as the Taklimakan, the NLLJ can extend to the meso and synoptic scales and may
100 couple to mid-tropospheric winds thus promoting long-range transport of dust
101 particles. A remarkable feature of the NLLJ is its breakdown after sunrise when the
102 NLLJ momentum is mixed to the surface, and thus wind speed near the surface is
103 greatly increased. The strong surface wind will resuspend dust particles from the
104 desert surface and the same turbulent mixing will also loft these dust to the upper
105 level of the boundary layer, promoting horizontal transport. Therefore, the NLLJ may
106 play an important role in the both dust emission and transport.

107 Much work has been done to address the features of the NLLJ, demonstrating a
108 link between NLLJs and dust suspension and their contribution to dust emission over



109 northern Africa [Allen and Washington, 2014; Fiedler et al., 2013; Washington and
110 Todd, 2005]. Since the TD has a hyper-arid environment and relative flat terrain,
111 strong radiative cooling during the night in this region must cause a stable near
112 surface layer and thus decouple the surface friction well. We may anticipate the IO is
113 the main NLLJ formation mechanism for this area. However, there have been very
114 few NLLJ studies over the Taklimakan region. Rife et al.[2010] examined the Tarim
115 basin NLLJ, but only focused on its diurnal variation for July. Du et al. [2014]
116 simulated diurnal variations of Tarim basin LLJs during early summer from 2006 to
117 2011 by using the Weather Research Forecast (WRF) model. In this paper, we present
118 an NLLJ detection algorithm and show the climatology and seasonal variation of
119 NLLJ over the Taklimakan by using the ERA-Interim reanalysis data. Satellite-based
120 aerosol optical depth (AOD) above the Taklimakan is also analyzed to explore the
121 effect of this NLLJ on dust emission from the desert surface.

122 **2. Data**

123 The essential data for the characterization of NLLJs over the TD is the latest
124 global atmospheric reanalysis fields of the ERA-Interim data on the model levels. It is
125 produced by European Centre for Medium-Range Weather Forecasts (ECMWF)
126 covering the data-rich period since 1979 and continuing in real time. Comparing with
127 the previous reanalysis data from ECMWF, the ERA-Interim has many substantial
128 improvements on the representation of the hydrological cycle, the quality of the
129 stratospheric circulation, and the handling of biases and changes in the observing
130 system [Dee et al., 2011]. The horizontal resolution of the data set is about 80 km



131 with 60 vertical levels from the surface up to 0.1 hPa. The 6-hourly daily wind speeds
132 and temperatures with a spatial resolution of $1^\circ \times 1^\circ$ from 2000 to 2013 were analyzed
133 in this study. We choose the ERA-Interim reanalysis for the climatological study of
134 NLLJs, because surface observations are very sparse due to the remoteness and harsh
135 environment of the TD and the ERA-Interim can provide sufficient vertical resolution.

136 Radiosonde data from two surface sites, Korla (86.08°E , 41.45°N) and Ruoqiang
137 (88.10°E , 39.02°N) (see Figure 1), were also used in this study. The radiosondes at
138 these two sites are launched at 08 and 20 Beijing time (BJT, eight hours ahead of
139 UTC) and have been operating more than 50 years. The quality controlled dataset is
140 updated through 2012. We compared ERA-Interim horizontal wind speed with
141 soundings at 00 UTC to validate reanalysis data.

142 The Multi-angle Imaging Spectro-Radiometer (MISR) onboard the Terra satellite,
143 which crosses the equator at 10:30 AM in its descending node, covers a swath of
144 approximately 360 km wide at the Earth's surface and obtains global coverage in
145 about 9 days. By taking advantage of the nine widely-spaced angles, MISR can
146 distinguish the top-of-atmosphere (TOA) reflectance contributions from the surface
147 and atmosphere, and successfully retrieve aerosol optical properties over bright
148 surfaces [Diner *et al.*, 2005]. In this study, we used level 3 daily AOD from 2000
149 through 2013 at 0.5° by 0.5° resolution to obtain the climatology of AOD and its
150 monthly variation over the Taklimakan.

151 3. Detection of NLLJs

152 The mean annual cycle of MISR-based AOD and ERA-Interim wind speed at 10 m



153 above surface, averaged over the TD region (see white box in Figure 1) for 2000-2013,
154 are shown in Figure 2. It is obvious that dust loading over the TD has a clear seasonal
155 variation. The AOD peaks in April and May with a monthly median value of ~ 0.5
156 while it decreases to a minimum in November and December with a monthly median
157 value of ~ 0.2 . We can also see that the AOD at 95 percentile for the month with
158 minimum median value can exceed 0.7, demonstrating that a large amount of dust can
159 be emitted over the TD throughout the year. The generation of dust aerosol, as well as
160 the consequent particle concentration, is highly dependent on the surface wind speed.
161 A study by Ge et al. [2014] has indicated a strong relationship between AOD and near
162 surface wind over this region. Figure 2 clearly shows that the monthly median value
163 of winds has the same trend as the AOD. Similar to the large spread of AOD, the
164 wind speed also has a wide range in each month.

165 Note that the annual mean circulation at 850 hPa (Figure 1) shows a band of high
166 wind speeds in the central Taklimakan. Figure 3 shows the vertical-latitudinal
167 distribution of annual mean wind speeds at 00 UTC (0600 local time) for the
168 longitudes of 82° , 85° and 88°E . It reveals that there is a maximum wind core centered
169 near 40°N at about 300-400 m AGL with a wind speed exceeding of 6.5 ms^{-1} . It can
170 extend over 10° in longitude and over 1° in latitude. Such night-time jet core occurs
171 widely and frequently over the TD. This phenomenon motivates us to examine the
172 details and climatology of NLLJs over the TD region and investigate the potential
173 effects of NLLJs on dust emission.

174 Before we use the ERA-Interim dataset to characterize the mesoscale episodes of



175 NLLJs occurring over the TD, it is necessary to validate the reanalysis data first. We
176 compared radiosonde data at the Ruoqiang and Korla sites with ERA-Interim winds at
177 the grids nearest to the observations sites during 2000 through 2012 when both the
178 reanalysis and validated sounding data are available. Figure 4 shows the comparison
179 of mean vertical wind speed profiles from reanalysis to a 13-year subset of sounding
180 data. We can see that the representation of the vertical wind structure in ERA-Interim
181 is reasonably good as compared with radiosondes. Importantly, the reanalysis data can
182 capture the elevation of the maximum low level winds, although ERA-Interim
183 underestimates the wind speed in the lower and middle atmosphere for the two sites.
184 We also compared the time series of wind speeds from reanalysis and radiosondes at
185 100 and 600 m AGL (not shown), and calculated the correlation coefficients and Root
186 Mean Square Errors (RMSE). Ruoqiang has a higher correlation coefficient that is
187 0.51 for the layer of 600 m AGL, while the RMSE of 4.9 ms^{-1} at Korla is about 0.5
188 ms^{-1} smaller than that at Ruoqing. Thus, we may expect that the ERA-Interim
189 adequately represents the wind structures over the TD.

190 In order to investigate the climatology of LLJs over the TD, a set of objective
191 criteria for automatically identifying their occurrences need to be specified. In the
192 literature, many criteria have been applied for identifying LLJs associated with
193 different formation mechanisms, data sets used and definitions of LLJ [Bonner, 1968;
194 Stull, 1988; Banta *et al.*, 2002; Baas *et al.*, 2009]. They include the range of
195 maximum wind height, threshold of wind speed at the jet core, and strength of vertical
196 wind shear. Here we developed an algorithm to detect the NLLJs from the



197 ERA-Interim reanalysis data by partly following the criteria given in Fiedler et al.
198 [2013] and Ranjha et al. [2013] where the ERA-Interim reanalysis data were used to
199 identify LLJs, and considering the IO mechanism of NLLJ formation. First, a
200 temperature inversion condition is identified and the inversion top height (H_i) is
201 determined by scanning each temperature profile. H_i must be above the third model
202 level, i.e. roughly 60 m (agl). This criterion generally assures that the lowest
203 atmospheric layers are stable and that the surface frictional drag on the air flowing
204 above it is reduced. Second, the maximum wind speed below 1500 m agl and its
205 height (H_j) are determined. The jet heights are confined to less than 1500 m following
206 Fiedler et al.[2013]. However, reducing this criterion to 900 m decreases the NLLJ
207 occurrence frequency by only 1 percent. Third, a wind speed minimum must exist
208 above the NLLJ but below 5 km agl with a value 60% or less relative to the wind
209 speed of the jet core. This condition is a combination and simplification of the second
210 and third criteria proposed by Ranjha et al. [2013], which is a description of LLJ wind
211 shear and ensures that identified NLLJs always have jet-like profiles. The use of a
212 relative threshold instead of a fixed one can provide a consistency in the detection of
213 the NLLJs that may have different strength in different seasons and weather
214 conditions.

215 **4. Climatology of NLLJs**

216 By applying these criteria to the 14-year ERA-Interim data, we found that the NLLJ
217 commonly appears over the Taklimakan and other adjacent arid regions. Figure 5
218 shows the monthly mean frequency of NLLJs for the TD and surrounding areas along



219 with contours of jet core speed. It is interesting to note that the NLLJs occurrence
220 frequency distribution derived from this identification method is closely related to the
221 topography and land surface type. One can see that the main feature of Figure 5 is a
222 frequency mode with values greater than 60% appearing in the entire Tarim Basin
223 throughout the year. The geographical distribution of NLLJs can extend eastward
224 from the main mode over the TD to the Loss Plateau along the north slope of the
225 Tibetan Plateau with decreasing frequency of occurrence toward the east. There are
226 also two other high frequency modes located near the TD region. One is in the Jungar
227 Basin located in northern Xinjiang which is a semi-arid area. The other is over desert
228 centered at 76°E, 46°N in Kazakhstan. Figure 5 reveals that our jet detection
229 algorithm is reliable. The NLLJ is a frequent, thus an important mesoscale weather
230 phenomenon over the TD and adjacent desert basins.

231 Figure 6 shows the climatological statistics of (a) jet height, (b) core speed, (c)
232 seasonal variation and (d) jet direction. Typically, the NLLJ occurs in a very shallow
233 layer. About 67% of the jet cores are located between 120 and 400 m AGL. 75% of
234 the jet core speeds fall between 4 and 10 ms⁻¹. The median values of the jet height and
235 jet core speed are 269 m and 6 ms⁻¹, respectively. By comparison, the median values
236 of the NLLJ height and core speed derived from ERA-Interim data for North Africa
237 [Fiedler, *et.al.*, 2013] are at 350 m and 10 ms⁻¹, which are higher and greater than
238 those over the Taklimakan, respectively. Figure 6c illustrates the monthly
239 climatology of jet height, jet core maximum speed and inversion height. We can see
240 that all these three parameters have clear seasonal variations. The jet speed generally



241 follows the trend of jet height that increases gradually from cold season to warm
242 season and has a maximum in August. The tendency for stronger LLJs to occur at
243 higher levels is the same as those found in other places [Banta *et al.*, 2002; Baas *et al.*,
244 2009; Fiedler *et al.*, 2013]. According to Blackadar's classical theory of IO
245 [Blackadar, 1957], the nocturnal inversion plays an important role in reducing eddy
246 viscosity and decoupling the air aloft in the planetary boundary layer from the surface
247 boundary layer. It thus causes a frictionless layer at the top of the inversion which is
248 the initial condition for the formation of NLLJ. However, we note that the jet can be
249 found at different heights which could be above the inversion top or embedded in the
250 inversion layer [Andreas *et al.*, 2000; Baas *et al.*, 2009]. Figure 6c shows that the
251 inversion height has an opposite seasonal trend to that of jet height. The inversion
252 height has minimum values in summer season, and can be as thick as 600 m in later
253 fall and winter which is much higher than the jet height of about 230 m. Our analysis
254 indicates that about half of the identified NLLJ cores are above the top of inversion
255 and the other half were embedded or partially embedded in the inversion layer. The
256 low solar elevation angle and high desert surface reflectivity during the cold season
257 would result in less sensible heat and thus a shallower day-time boundary layer but a
258 strongly stable nocturnal boundary layer. In these cases the NLLJ occurs a few
259 hundred meters above the surface where the layer is well stratified and the NLLJ
260 winds are decoupled from the surface friction layer.

261 The wind rose in figure 6d shows that the prevailing wind direction of the jet core
262 is narrowly distributed between east-northeast and east-southeast, 67 percent of



263 NLLJs over all seasons are within the four sectors between 40 and 120 degrees. This
264 narrow angular NLLJ directional distribution is mainly confined by the topography.

265 **5. NLLJ effects on dust emission**

266 Considering that the emission of dust initially develops in the surface boundary
267 layer and is proportional to third or fourth power of the surface wind speed, it is
268 expected that the NLLJ can affect dust production if we can find that NLLJ do have
269 impacts on near surface wind speed and variability. Recent studies [*Christopher &*
270 *Washington, 2014; Heinold et al., 2013; Knippertz, 2008; Schepanski et al., 2009*]
271 have indicated that the breakdown of the NLLJ over Africa can induce the downward
272 mixing of momentum during the evolution of the boundary layer in mid-morning and
273 cause enhancement of near surface wind speed. Here, we firstly compared the
274 mid-morning surface wind speed distribution coincident with the appearance of NLLJ
275 with that when no NLLJ was detected. Ideally this would have been calculated for
276 10:00 AM local time to observe the maximum effect but only 6-hourly ERA data
277 were available. Figure 7 shows the near surface wind speed frequency distribution at
278 06 UTC (i.e., 11:30 AM local time) over the Taklimakan. We can see an obvious shift
279 of wind speed toward higher values when NLLJs are present compared to the days
280 when there is no NLLJ. This result may be an evidence of NLLJ effects on surface
281 wind speed and a link between NLLJs and dust emission. However, if we take a
282 further look at the detailed behavior of near surface wind speed difference between jet
283 and non-jet days for the seasonal cycle over the Tarim basin, the spatial distributions
284 of wind speed difference of each month are substantially different. In Figure 8, we can



285 see that positive differences are dominant in the basin during cold season from
286 October to March, but negative values are distributed over the most basin area with
287 only a weak positive belt aligning along the north slope of the Tibet Plateau during
288 April to September. This seasonal contrast in the surface wind speed difference is
289 exactly coincident with the relative position of jet height and inversion height that are
290 shown in Figure 6c. As we know, a convective boundary layer starts with morning
291 insolation, grows gradually to dissipate the nocturnal surface inversion and transport
292 momentum from aloft to the surface. However, this process could be either very rapid
293 or much slower depending on solar heating and other meteorological conditions. We
294 may expect when the inversion layer is much thicker and the surface heating is very
295 weak in the cold season, the development of mixed layer may be very slow and the
296 unstable layer happens to reach the height of NLLJ at 06 UTC. Thus momentum from
297 the LLJ is mixed down and leads to an increase of the surface wind speed, showing a
298 positive difference during these months. By contrast in the warm season, a mixed
299 boundary layer is developed very rapidly, LLJ momentum transport process may have
300 been already largely completed by 06 UTC. The surface friction is well coupled with
301 boundary layer and consumes the downward momentum, eventually leads to a
302 sub-geostrophic wind.

303 To test this hypothesis, we need to further investigate the height of convective
304 boundary layer (CBL) in the mid-morning (06 UTC). The Richardson number (Ri)
305 that indicates the dynamic instability of the flow is used here to determine the
306 CBL height. The Ri is a measure of relative strength of buoyance and mechanical



307 wind shear. It is defined as:

$$R_i = \frac{\frac{g}{\theta} \left(\frac{\partial \theta}{\partial z} \right)}{\left(\frac{\partial u}{\partial z} \right)^2 + \left(\frac{\partial v}{\partial z} \right)^2}$$

308 where θ is the potential temperature, g is the acceleration of gravity, z is the height,
309 and u and v are the horizontal wind velocity components. Clearly, turbulent energy
310 increases when $R_i < 1$, but theoretical and experimental studies show that
311 non-turbulent flow becomes turbulent when R_i drops below a critical value of around
312 0.25. We first selected those profiles in which the potential temperature at the lowest
313 level is larger than at the next higher level to ensure that the turbulence is induced by
314 surface heating. Then we calculated the R_i numbers between successive levels for the
315 selected profiles, and searched each profile from the surface upwards, and defined the
316 lowest level, where R_i value exceeds the critical value of 0.25, as the top of the CBL.
317 The red lines in Figure 9 plot the monthly variations of the CBL height at 06 UTC
318 averaged on days with and without NLLJ over the TD. The variations for both jet and
319 no jet cases exhibit the same tendency that the greatest heights appear in June and the
320 lowest heights of about 200 m occur in December and January. Obviously, the
321 tendencies are primarily a response to the solar insolation which drives the local
322 thermal forcing and the terrestrial cooling. During cold season from October to March,
323 the monthly mean CBL heights on jet days are almost the same as those on no jet days,
324 and close to the jet core height. Significant differences in CBL heights between jet
325 and non-jet days are evident in the months from April to September. This is because in
326 the warm season only on cloudless nights can a large amount of thermal radiation



327 escape to space and allow intensive radiative cooling to form a stable surface layer,
328 leading to the development of NLLJ aloft. In midmorning, cloudless conditions also
329 allow more solar radiation to reach at the surface and thus cause a stronger surface
330 heating that consequently induces a stronger turbulence and a higher mixed layer than
331 non-jet days. We may infer that stronger vertical mixing on days with jet occurrence
332 can transport momentum between the surface and a given height in or above the stable
333 layer rapidly in the warm season.

334 Having quantified the CBL height, we next quantified the magnitude of the
335 momentum in the boundary by constructing an index. It is a summation of wind speed
336 from the height just above the surface layer to the height of the CBL with a unit of
337 m^2s^{-1} :

$$\text{Index} = \int_{H_s}^{H_c} U(h) dh$$

338 where H_s is the top of the surface layer which is typically about 10% of the boundary
339 layer depth which we selected as the height of the third model level above the surface.
340 H_c is the top of the CBL that is derived from Ri and $U(h)$ is the wind speed profile.
341 We applied this index on each grid of the ERA-Interim at 00 UTC and averaged the
342 index values over the TD region. The blue lines in Figure 9 show the monthly
343 variations of the momentum index for days with and without NLLJ occurring at 00
344 UTC. The seasonal trends of the index are largely determined by the integral depth
345 (i.e. the height of the CBL) and thus vary consistently with the CBL height. More
346 importantly, the momentum index on days with NLLJs are always larger than those on
347 days without NLLJs even if there is no a big difference in H_c between jet and non-jet



348 cases. Note that for both NLLJ and non-NLLJ cases CBL heights during October
349 through March are almost the same but are significantly different during the warm
350 season. By combining the CBL height, momentum index and near surface wind speed
351 shown in Figure 8 and 9, we may draw a conclusion that at night the boundary layer
352 between H_s and H_c with NLLJ contains more momentum than without NLLJ. When
353 the NLLJ breaks down in midmorning its momentum is transported toward the
354 surface, decreasing the speed aloft but producing stronger surface winds. This process
355 is suppressed during cold season when the inversion depth is greater and consequently
356 results in less downward momentum transfer that occurs over a longer period of time.
357 In the summer season, the downward momentum transfer process is more intense and
358 rapid and could cause a significant increase in surface wind speed which is not
359 captured by the 6-hour ERA dataset.

360 The above investigation has indicated that the momentum in an upper boundary
361 layer is larger, and the turbulence is much stronger especially in summer for the NLLJ
362 cases than without NLLJ occurrence. A larger momentum and stronger transfer
363 consequently can lead to an enhancement of the surface wind speed. In order to find a
364 direct evidence of NLLJs effects on dust emission, a composite difference method is
365 used to analyze the relationship between NLLJ winds and dust generation. We point
366 out that if the wind profile composite is simply based on high and low dust loading,
367 an enhancement of wind in the lower atmosphere will always be seen because larger
368 wind speed is directly related to dust generation for a given surface condition. Thus,
369 there is a risk to evaluating the effect of NLLJ on dust emission since we cannot tell if



370 stronger surface winds are associated with the NLLJ. To avoid this risk, we select
371 only ERA-Interim data for which 80% of the grid points along the section at 40° N
372 between the latitudes of 78 and 88° E are identified with the appearance of NLLJ. We
373 then match the time series of the NLLJ data and AOD observations for the composite
374 analysis. According to the seasonal distribution of AOD, we use the 10 and 90
375 percentile values of the AOD cumulative distribution function to identify the most and
376 least dusty days and 42 samples for winter and 58 samples for each of the other three
377 seasons are picked out for the composite difference analysis. Figure 10 shows the
378 seasonal composite differences of latitudinal wind speed between the most and least
379 dusty days along 40° N. It is clear that the NLLJ is significantly enhanced on days of
380 high AOD for summer and autumn seasons and that the core speed increases by more
381 than 3 ms⁻¹. Due to stronger turbulent mixing in summer compared to other seasons,
382 NLLJ level winds may affect the surface wind speed and variance causing a deeper
383 surface layer with a significant increase of wind speed on high dust days in summer
384 than autumn.

385 We also notice an interesting phenomenon that although AOD values are highest
386 in spring (Figure 2), NLLJ speeds are not significantly higher in this season. It is well
387 known that cold frontal intrusions with high synoptic scale winds cause strong dust
388 storms in spring. Obviously our results indicate that occurrences of NLLJ have
389 relatively less influence on dust emission in the spring when synoptic scale winds
390 dominate dust resuspension.

391 6. Conclusion



392 In this study, we presented a long-term, detailed structure of the wind profile in the
393 atmospheric boundary layer over the Taklimakan Desert which has a relative flat
394 terrain. A comparison of radiosondes and ERA-Interim reanalysis at two sites in the
395 Tarim basin shows that the reanalysis data can capture the feature of the low level
396 wind profile. Based on our NLLJ detection algorithm, NLLJs are frequent over the
397 entire Tarim Basin and Taklimakan Desert throughout the entire year with an
398 occurrence frequency above 60%. The dominant wind directions are east and
399 east-northeast in all seasons. The annual mean values of jet height and core speed are
400 270 m and 6 ms^{-1} , respectively. The jet core height and speed show seasonal
401 variations, both with maximum values in August and minimum in January. The
402 inversion height also changes with season, but in a manner opposite to the height of
403 the jet core. We found that about 50% of the identified NLLJ cores are above the top
404 of inversion (more frequently in the warmer season), and the other half of NLLJs was
405 embedded in the inversion layer (mostly in the colder season).

406 The midmorning breakdown of the nocturnal inversion and jet core are remarkable
407 and consistent features of NLLJ over the TD. The momentum of these NLLJ can be
408 mixed downward, increasing surface wind speed, which could be the driving
409 mechanism for dust emission over this and other arid regions. We calculated the CBL
410 height, and construct an index to quantify the magnitude of the momentum from the
411 top of the surface layer to the CBL height. It is found that the momentum in an upper
412 boundary layer is larger for the NLLJ cases than without NLLJ occurrence in all
413 seasons, while the CBL heights in warm season are much greater than those in cold



414 season. This indicates that stronger vertical mixing on days with jet occurrence can
415 transport more momentum between the surface and CBL height in the warm season,
416 enhancing the surface wind speed.

417 We further match the NLLJ and MISR AOD data and found that there was a
418 significant enhancement of NLLJ during high AOD days in summer and autumn
419 seasons when the core speed increased by more than 3 ms^{-1} . In the colder season, the
420 sensible heat energy input is much less and the inversion layer is thicker which
421 suppresses the downward propagation of turbulence, thus NLLJs have a lesser effect
422 on surface wind and dust emission in winter and spring.

423 Nocturnal low-level jets have been identified as a frequent mesoscale phenomenon
424 over the TD and are possibly an important mechanism for dust emission especially in
425 the summer months. To define the details of the NLLJ diurnal cycle and to clarify the
426 causal and quantitative relationships to dust emission and transport, further
427 ground-based in-situ and remote sensing measurements of winds and dust
428 concentration profiles are needed along with high spatial and temporal resolution
429 numerical modeling.

430

431 Data availability: The data for this paper are available at NASA Atmospheric Data
432 Center and ECMWF. Data sets: MISR, ERA Interim. Date name:
433 MIL3DAE_*.004_*.hdf, ERA_Interim_*.nc

434 *Acknowledgements:* This work was supported by the National Science Foundation of
435 China (41275070, 41521004, 41575016), China 111 project (No.B 13045), and the
436 Fundamental Research Funds for the Central University (Izujbky-2015-K02). We
437 thank Prof. Dave S. Covert for useful comments and discussion.



- 438 References
- 439 Allen, C. J. T., and R. Washington (2014), The low-level jet dust emission mechanism
- 440 in the central Sahara: Observations from Bordj-Badji Mokhtar during the June 2011
- 441 Fennec Intensive Observation Period, *J. Geophys. Res. Atmos.*, 119(6), 2990-3015.
- 442 Andreas, E. L., K. J. Claffy, and A. P. Makshtas (2000), Low-level atmospheric jets
- 443 and inversions over the western Weddell Sea, *Bound. Lay. Meteorol.*, 97(3), 459-486.
- 444 Baas, P., F. C. Bosveld, H. K. Baltink, and A. A. M. Holtslag (2009), A Climatology
- 445 of Nocturnal Low-Level Jets at Cabauw, *J. Appl. Meteorol. Climatol.*, 48(8),
- 446 1627-1642.
- 447 Banta, R. M., R. K. Newsom, J. K. Lundquist, Y. L. Pichugina, R. L. Coulter, and L.
- 448 Mahrt, 2002: Nocturnal low-level jet characteristics over Kansas during CASES-99.
- 449 *Bound.-Layer Meteor.*, 105, 221–252.
- 450 Blackadar, A. K. (1957), Boundary layer wind maxima and their significance for the
- 451 growth of nocturnal inversions, *Bull. Amer. Meteor. Soc.*, 283-290.
- 452 Bonner, W. D., (1968), Climatology of the low level jet. *Mon. Wea.Rev.*, 96, 833–
- 453 850.
- 454 Chen, S., J. Huang, C. Zhao, Y. Qian, L. R. Leung, and B. Yang (2013), Modeling the
- 455 transport and radiative forcing of Taklimakan dust over the Tibetan Plateau: A case
- 456 study in the summer of 2006, *J. Geophys. Res. Atmos.*, 118(2), 797-812.
- 457 Dee, D. P., et al. (2011), The ERA-Interim reanalysis: configuration and performance
- 458 of the data assimilation system, *Quart. J. Roy. Meteorol. Soc.*, 137(656), 553-597.
- 459 Diner, D. J., J. V. Martonchik, R. A. Kahn, B. Pinty, N. Gobron, D. L. Nelson, and B.
- 460 N. Holben (2005), Using angular and spectral shape similarity constraints to improve



- 461 MISR aerosol and surface retrievals over land, *Remote Sens. Environ.*, 94(2),
462 155-171.
- 463 Du, Y., Q. Zhang, Y.-L. Chen, Y. Zhao, and X. Wang, (2014), Numerical simulations
464 of spatial distributions and diurnal variations of low-level jets in China during early
465 summer. *J. Climate*, 27,5748–5767, doi:10.1175/JCLI-D-13-00571.1.
- 466 Fiedler, S., K. Schepanski, B. Heinold, P. Knippertz, and I. Tegen (2013), Climatology
467 of nocturnal low-level jets over North Africa and implications for modeling mineral
468 dust emission, *J. Geophys. Res. Atmos.*, 118(12), 6100-6121.
- 469 Fu, Q., T. J. Thorsen, J. Su, J. M. Ge, and J. P. Huang (2009), Test of Mie-based
470 single-scattering properties of non-spherical dust aerosols in radiative flux
471 calculations, *J. Quant. Spectrosc. Radiat. Transf.*, 110(14-16), 1640-1653.
- 472 Ge, J. M., J. P. Huang, C. P. Xu, Y. L. Qi, and H. Y. Liu (2014), Characteristics of
473 Taklimakan dust emission and distribution: A satellite and reanalysis field perspective,
474 *J. Geophys. Res. Atmos.*, 119, doi:10.1002/2014JD022280.
- 475 Ge, J. M., J. P. Huang, J. Su, J. R. Bi, and Q. Fu (2011), Shortwave radiative closure
476 experiment and direct forcing of dust aerosol over northwestern China, *Geophys. Res.*
477 *Lett.*, 38.
- 478 Ge, J. M., J. Su, T. P. Ackerman, Q. Fu, J. P. Huang, and J. S. Shi (2010), Dust aerosol
479 optical properties retrieval and radiative forcing over northwestern China during the
480 2008 China-US joint field experiment, *J. Geophys. Res. Atmos.*, 115.
- 481 Heinold, B., P. Knippertz, J. H. Marsham, S. Fiedler, N. S. Dixon, K. Schepanski, B.
482 Laurent, and I. Tegen (2013), The role of deep convection and nocturnal low-level



483 jets for dust emission in summertime West Africa: Estimates from
484 convection-permitting simulations, *J. Geophys. Res. Atmos.*, 118, 4385–4400,
485 doi:10.1002/jgrd.50402.

486 Huang J., Yu H., Guan X., Wang G. and Guo R., 2015: Accelerated dryland expansion
487 under climate change, *Nature Climate Change*, doi:10.1038/nclimate2837.

488 Huang, J., T. Wang, W. Wang, Z. Li, and H. Yan, 2014: Climate effects of dust
489 aerosols over East Asian arid and semiarid regions, *J. Geophys. Res.: Atmospheres*,
490 119, 11398–11416, doi:10.1002/2014JD021796.

491 Huang, J., Q. Fu, J. Su, Q. Tang, P. Minnis, Y. Hu, Y. Yi, and Q. Zhao (2009),
492 Taklimakan dust aerosol radiative heating derived from CALIPSO observations using
493 the Fu-Liou radiation model with CERES constraints, *Atmos. Chem. Phys.*, 9(12),
494 4011-4021.

495 Huang, J., P. Minnis, B. Chen, Z. Huang, Z. Liu, Q. Zhao, Y. Yi, and J. K. Ayers, 2008:
496 Long-range transport and vertical structure of Asian dust from CALIPSO and surface
497 measurements during PACDEX, *J. Geophys. Res.*, 113, D23212,
498 doi:10.1029/2008JD010620.

499 Huang, J., P. Minnis, Y. Yi, Q. Tang, X. Wang, Y. Hu, Z. Liu, K. Ayers, C. Trepte, and
500 D. Winker (2007), Summer dust aerosols detected from CALIPSO over the Tibetan
501 Plateau, *Geophys. Res. Lett.*, 34(18).

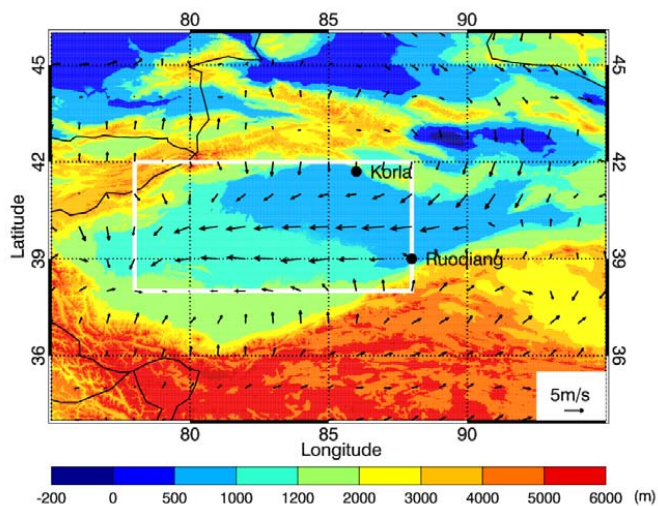
502 Ling, X., W. Guo, C. Fu (2014), Composite analysis of impacts of dust aerosols on
503 surface atmospheric variables and energy budgets in a semiarid region of China, *J.*
504 *Geophys. Res. Atmos.*, 119, 3107–3123, doi:10.1002/2013JD020274



- 505 Knippertz, P. (2008), Dust emissions in the West African heat trough the role of the
506 diurnal cycle and of extratropical disturbances, *Meteorol. Z.*, 17(5), 553–563,
507 doi:10.1127/0941-2948/2008/0315.
- 508 Lohmann, U., and J. Feichter (2005), Global indirect aerosol effects: A review, *Atmos.*
509 *Chem. Phys.*, 5, 715–737, doi:10.5194/acp-5-715-2005.
- 510 Ranjha, R., G. Svensson, M. Tjernström, and A. Semedo, (2013), Global distribution
511 and seasonal variability of coastal low level jets derived from ERA-Interim reanalysis.
512 *Tellus*, 65A, 20412, doi:10.3402/tellusa.v65i0.20412.
- 513 Rife, D. L., J. O. Pinto, A. J. Monaghan, C. A. Davis, and J. R. Hannan (2010), Global
514 Distribution and Characteristics of Diurnally Varying Low-Level Jets, *J. Climate*,
515 23(19), 5041-5064.
- 516 Shao, Y., K.-H. Wyrwoll, A. Chappell, J. Huang, Z. Lin, G. H. McTainsh, M. Mikami,
517 T. Y. Tanaka, X. Wang, and S. Yoon (2011), Dust cycle: An emerging core theme in
518 Earth system science, *Aeolian Res.*, 2(4), 181-204.
- 519 Stensrud, D. J. (1996), Importance of low-level jets to climate: A review, *J. Climate*,
520 9(8), 1698-1711.
- 521 Stull, R. B., (1988), *An Introduction to Boundary Layer Meteorology*. Kluwer
522 Academic, 666 pp.
- 523 Schepanski, K., I. Tegen, M. C. Todd, B. Heinold, G. Bönisch, B. Laurent, and A.
524 Macke (2009), Meteorological processes forcing Saharan dust emission inferred from
525 MSG-SEVIRI observations of subdaily dust source activation and numerical models,
526 *J. Geophys. Res. Atmos.*, 114, D10201, doi:10.1029/2008JD010325.



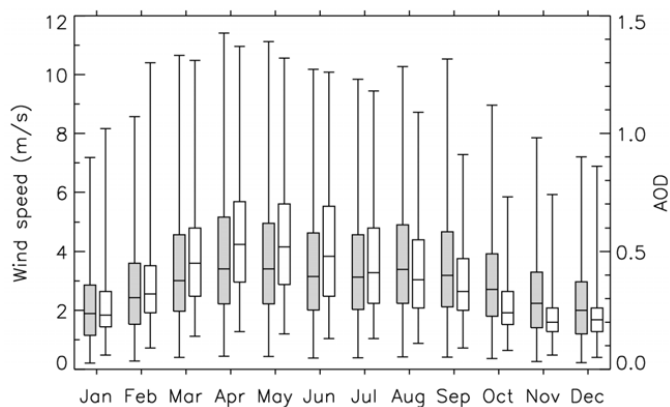
- 527 Su, J., J. Huang, Q. Fu, P. Minnis, J. Ge, and J. Bi (2008), Estimation of Asian dust
528 aerosol effect on cloud radiation forcing using Fu-Liou radiative model and CERES
529 measurements, *Atmos. Chem. Phys.*, 8(10), 2763-2771.
- 530 Sun, J. M., M. Y. Zhang, and T. S. Liu (2001), Spatial and temporal characteristics of
531 dust storms in China and its surrounding regions, 1960-1999: Relations to source area
532 and climate, *J. Geophys. Res. Atmos.*, 106(D10), 10325-10333.
- 533 Uno, I., K. Eguchi, K. Yumimoto, T. Takemura, A. Shimizu, M. Uematsu, Z. Liu, Z.
534 Wang, Y. Hara, and N. Sugimoto (2009), Asian dust transported one full circuit
535 around the globe, *Nat. Geosci.*, 2(8), 557-560.
- 536 Van de Wiel, B. J. H., A. F. Moene, G. J. Steeneveld, P. Baas, F. C. Bosveld, and A. A.
537 M. Holtslag (2010), A Conceptual View on Inertial Oscillations and Nocturnal
538 Low-Level Jets, *J. Atmos. Sci.*, 67(8), 2679-2689.
- 539 Washington, R., and M. C. Todd (2005), Atmospheric controls on mineral dust
540 emission from the Bodele Depression, Chad: The role of the low level jet, *Geophys.*
541 *Res. Lett.*, 32(17).



542

543 Figure 1. Map of the Taklimakan Desert region with its topography and annual mean

544 wind at 850 hPa.



545

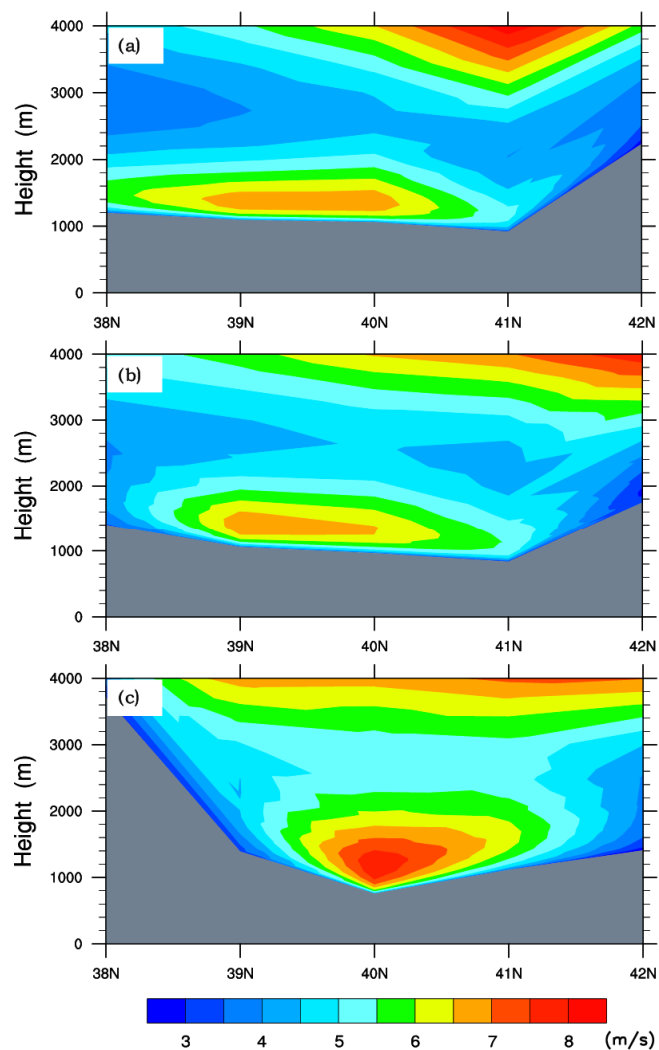
546

547 Figure 2. Annual cycles of wind speed (gray bars) and AOD (white bars) from 2000

548 through 2013 over the Taklimakan Desert. The horizontal line through each box

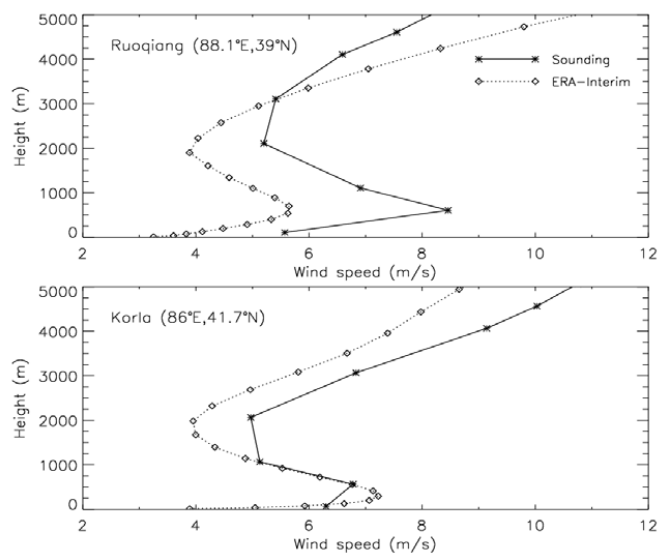
549 represents that monthly median value; top and bottom of the boxes mark 75% and 25%

550 percentiles, respectively; whiskers mark the 95% and 5% percentiles.



551

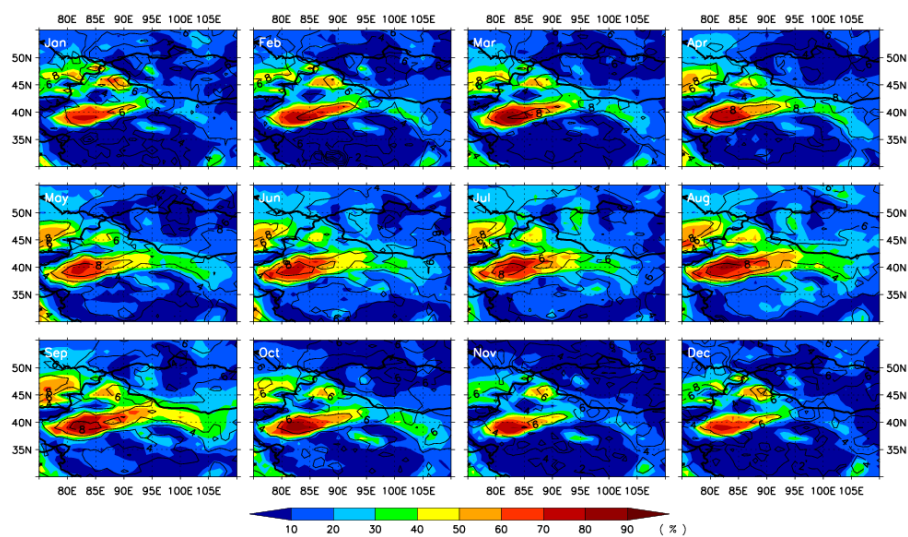
552 Figure 3. Latitude-height cross sections of annual mean wind speed at three
553 longitudes of (a) 82 ° E, (b) 85° E, and (c) 88 ° E from ERA-Interim reanalysis
554 averaged over 2000-2013. Gray areas represent the terrain elevation.



555

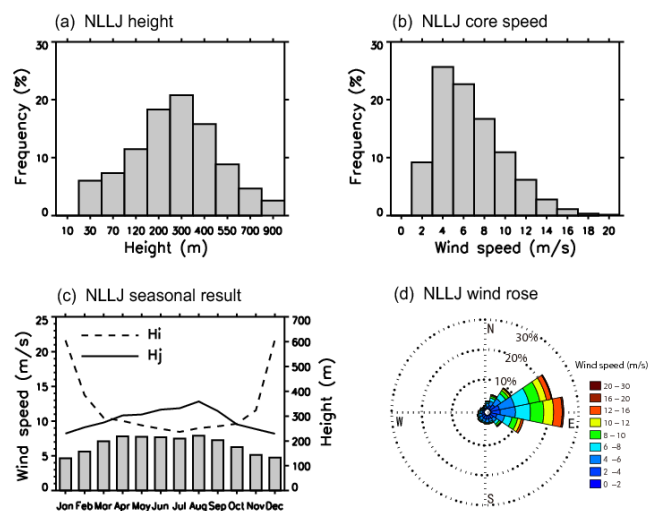
556 Figure 4. Mean wind speed profiles at 00 UTC based on radiosondes (solid line) and

557 ERA-Interim (dot line) at (a) Ruoqiang and (b) Korla sites for 2000 - 2012.



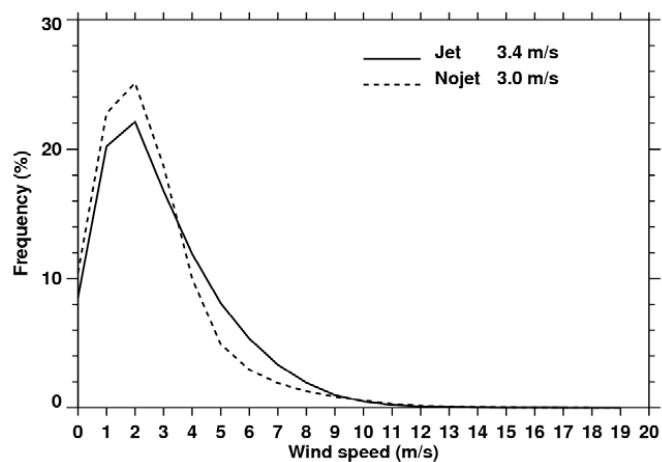
558

559 Figure 5. Monthly mean occurrence of the NLLJ frequency (colors) with jet core wind
560 speed (contours) at 00 UTC by applying the NLLJ detection algorithm to the
561 ERA-Interim reanalysis data for 2000-2013.



562

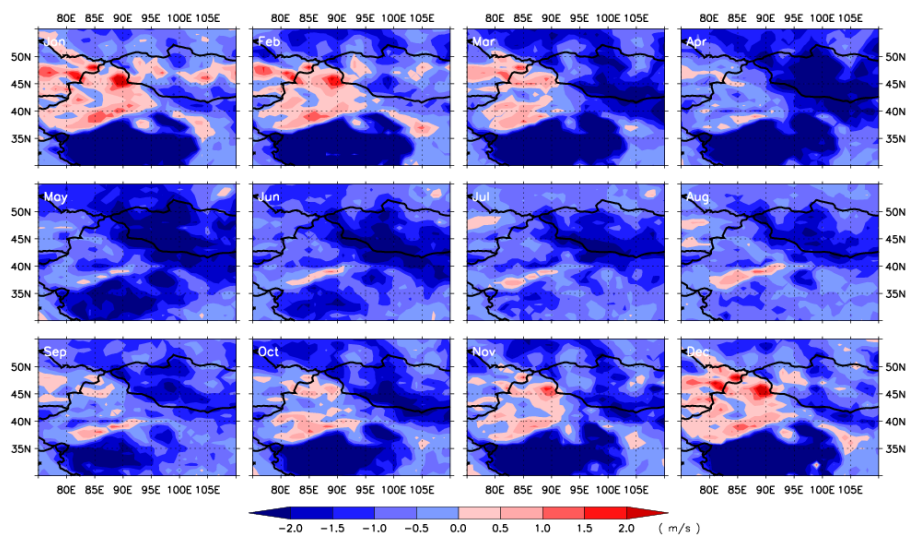
563 Figure 6. Climatological features of NLLJ over the Tarim Basin (38°-42° N, 78°-88°
564 E). (a) Frequency distribution of NLLJ height. (b) Frequency distribution of NLLJ
565 speed. (c) Monthly mean jet core speed (gray bar), NLLJ core height (solid line) and
566 inversion height (dashed line). (d) Jet core wind direction and speed distribution at 00
567 UTC (i.e., 0530 local) from ERA-Interim reanalysis from 2000 through 2013.



568

569 Figure 7. Frequency distribution of 10 m wind speed at 06 UTC (i.e. roughly at 1130

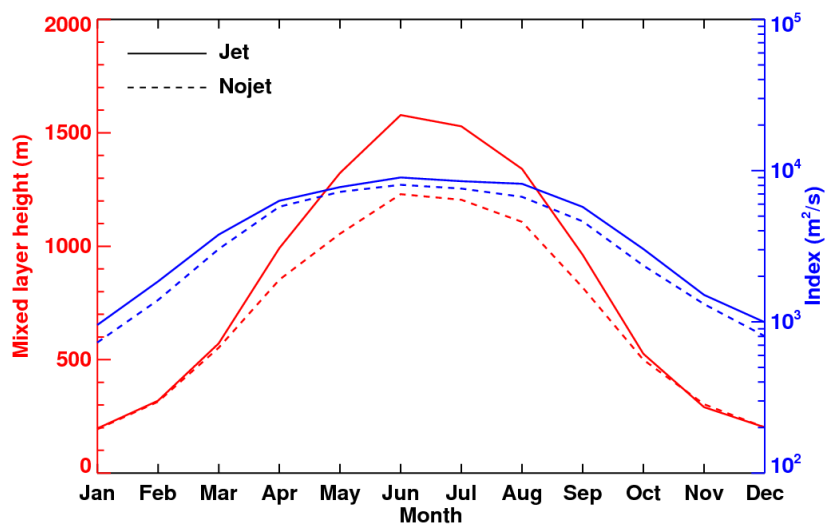
570 local time) over the Tarim basin.



571

572 Figure 8. Annual cycle of the near surface wind speed difference at 06 UTC between

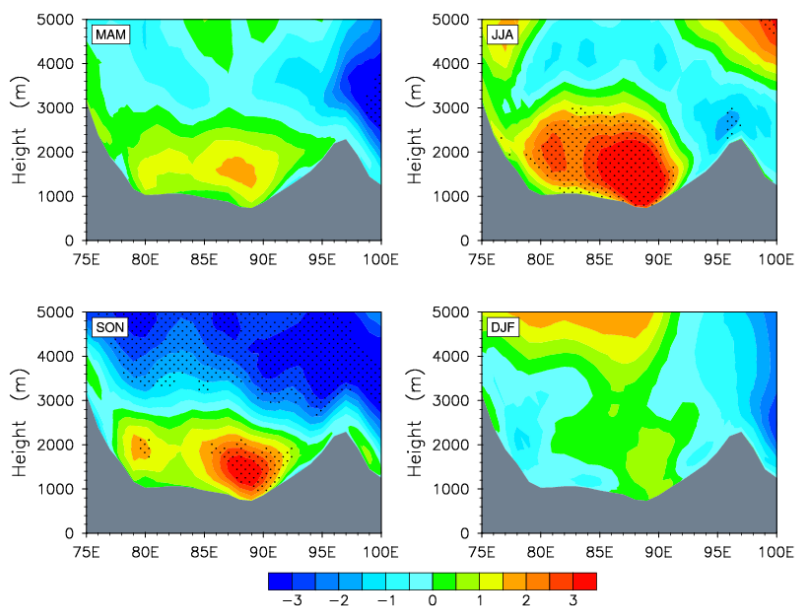
573 NLLJ and non-NLLJ days.



574

575 Figure 9. Monthly-averaged convection boundary layer height at 06 UTC, and

576 momentum index at 00 UTC over the TD.



577

578 Figure 10. Seasonal longitudinal cross-sections of daily wind composite difference

579 between high and low AOD days along 40° N. Stippled areas are significant at the 95%

580 level. Gray areas represent terrain.